

Design and Modeling of a High-Speed AFM-Scanner

Georg Schitter, *Member, IEEE*, Karl J. Åström, *Fellow, IEEE*, Barry E. DeMartini, *Member, IEEE*, Philipp J. Thurner, Kimberly L. Turner, and Paul K. Hansma

Abstract—A new mechanical scanner design for a high-speed atomic force microscope (AFM) is presented and discussed in terms of modeling and control. The positioning range of this scanner is $13\ \mu\text{m}$ in the X - and Y -directions and $4.3\ \mu\text{m}$ in the vertical direction. The lowest resonance frequency of this scanner is above 22 kHz. This paper is focused on the vertical direction of the scanner, being the crucial axis of motion with the highest precision and bandwidth requirements for gentle imaging with the AFM. A second- and a fourth-order mathematical model of the scanner are derived that allow new insights into important design parameters. Proportional–integral (PI)-feedback control of the high-speed scanner is discussed and the performance of the new AFM is demonstrated by imaging a calibration grating and a biological sample at 8 frames/s.

Index Terms—Atomic force microscopy, fast scanning, mechatronics, nanotechnology, precision positioning, real time imaging.

I. INTRODUCTION

THE ATOMIC force microscope (AFM) [1] is a very important instrument for exploring materials at the scale of a few nanometers [2]. The principle of the AFM is to raster scan a sample in close vicinity to a probing tip that is mounted on the free end of a micromechanical cantilever. The deflection of this cantilever can be measured with subnanometer precision [3]. A feedback controller tracks the probing force by varying the position of the sample in the vertical direction. Thus, the output of the feedback controller corresponds to the height of the topographical feature on the corresponding lateral position in the plane of the raster scan. To avoid damages to the sample or the tip, it is desirable to use a small force, particularly when imaging biological specimens. A high-performance feedback controller is required in order to minimize variations of the imaging force

and to avoid loss of the tip sample contact due to a decline in the sample surface.

The scanning speed of current AFM systems is limited due to the dynamic behavior of the individual microscope components. The main limitations are 1) the response time of the force sensor [4], 2) the dynamic behavior of the scanning unit [5], [6], 3) the bandwidth of the feedback loop that controls the interaction force between the tip and the sample [7], and 4) the speed of the data acquisition system [8], [9]. Some efforts have been made to speed up imaging by using smaller and faster force sensors [10], [11] and directly actuated cantilevers [12], [13], by improving the mechanical design of the scanner [14]–[16], by exploiting alternative scanning methods [17], and by utilizing advanced control methods for faster scanning [5], [6], [18]–[22] and faster vertical motion [7], [23], [24]. Parallel operation of several AFM probes has also been successfully implemented [25], [26].

In spite of all previous advances there are still needs and possibilities to improve system performance, particularly in the vertical (Z) direction, which is the control task with the highest requirements on bandwidth and precision.

From a control engineering point of view, the sample topography acts as a disturbance to the AFM in Z -direction, that has to be compensated by the feedback controller [23]. For AFM imaging usually no oscillations in the control action and in the cantilever deflection are required to keep image distortion at a minimum. This is achieved by setting the control bandwidth sufficiently low, which contradicts with the requirement of a high bandwidth for gentle imaging. However, recent developments reported methods that enable faster imaging without distortions by utilizing advanced control techniques [7], [27]. The oscillatory modes of the AFM system are compensated by the controller and the undistorted topography information is then obtained by model-based filtering of the high-bandwidth control action.

This paper presents a new mechanical scanner design that allows scanning speeds that are more than two orders of magnitude faster than current commercial AFM systems. The goal is to develop a high-performance system by combined process and control design. We analyze the vertical motion of the new scanner, where the motivation is to gain detailed insights into the system dynamics and to understand how process design influences the control design. Section II presents the mechanical design of the new scanner. A mathematical model of the scanner based on first principles is derived in Section III and experimentally verified in Section IV. Feedback operation of the high-speed AFM is discussed (see Section V) and the performance of the new AFM is demonstrated by imaging a biological sample.

Manuscript received February 27, 2006; revised October 31, 2006. Manuscript received in final form February 5, 2007. Recommended by Guest Editor E. Eleftheriou. This work was supported in part by the National Science Foundation through the UCSB Materials Research Laboratory under Award DMR00-80034 and Award NSF SST ECS04-28916, by the National Institutes of Health under Award RO1 GM 065354-05, by the NASA University Research, Engineering, and Technology Institute on Bio-inspired Materials under Award NCC-1-02037, by a research agreement with Veeco #SB030071, by the SNF Project PA002-108933, and the SNF Project PA002-111445.

G. Schitter is with Delft University of Technology, Delft Center for Systems and Control, 2628 CD, Delft, The Netherlands (e-mail: g.schitter@tudelft.nl)

K. J. Åström, B. E. DeMartini, and K. L. Turner are with the Department of Mechanical and Environmental Engineering, University of California, Santa Barbara, CA 93106 USA (e-mail: astrom@engineering.ucsb.edu; baredog@uemail.ucsb.edu; turner@engineering.ucsb.edu).

P. J. Thurner and P. K. Hansma are with the Department of Physics, University of California, Santa Barbara, CA 93106 USA (e-mail: thurner@physics.ucsb.edu; prasant@physics.ucsb.edu).

Color versions of one or more of the figures in this paper are available online at <http://ieeexplore.ieee.org>.

Digital Object Identifier 10.1109/TCST.2007.902953

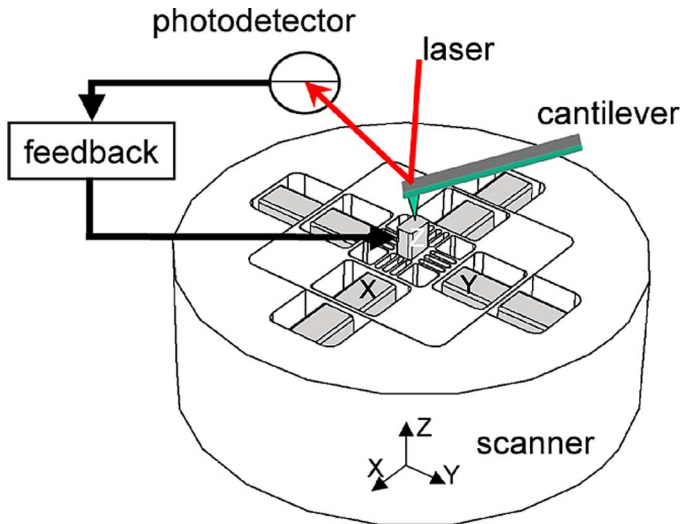


Fig. 1. Scheme of the high-speed scanner including the feedback loop to track the tip-sample interaction force for gentle imaging. The Z -piezo sits on top of the center cube that is moved laterally by the scanning piezos and flexure structure.

II. SCANNER DESIGN

The scanner is the core unit of the new high-speed AFM, enabling faster imaging by improved performance and bandwidth. The most important design goal for the new scanner was to combine the individual actuators into a 3-D positioner with the lowest resonance frequency as high as possible, preferably above 20 kHz, for a fast response.

A. Mechanical Design

The new scanner design is based on piezoelectric stack actuators (piezos) and a flexure mechanism that enables decoupling of the different axes of motion while keeping the mechanical structure stiff (see Fig. 1). The key element in this design is to make the scanner compact and rigid [15], i.e., to make the mechanical paths as short as possible, in order to achieve high first-resonance frequencies in all positioning directions. The Z -actuator (for vertical positioning) is mounted on a center piece that is moved by the X and Y piezos (for lateral positioning). The small parallel flexures that connect the center piece with the inner frame decouple the X and Y motion. The inner frame, that is connected to the support material and sits between the parallel flexures and the scanning piezos, is flexible in the actuation direction of the respective piezo and is stiff in the two perpendicular directions. This confines the possible movement of the piezo to its actuation direction and suppresses out of plane and screw-like motion of the respective actuator. Simultaneously, this inner frame also serves as rigid support of the Z -actuator by reducing the mechanical path length of the Z -actuator's support. The second flexure frame that is located between the inner and outer pairs of the scanning piezos plays the same role. This combination of flexures results in a shift of the first resonance frequency in the Z -direction towards much higher frequencies and suppresses trampoline motion of the scanning system in the Z -direction. For actuation in the scanning directions (X and Y) this scanner is built in the so-called "push-pull

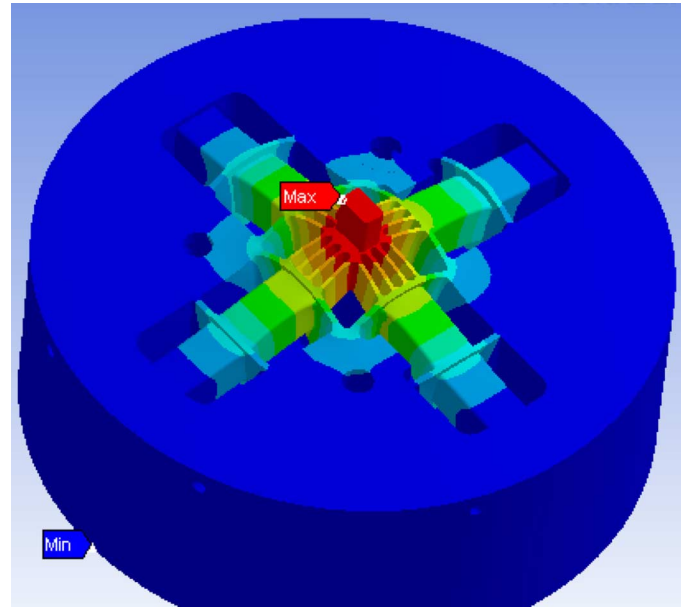


Fig. 2. FEA of the high-speed scanner exaggeratedly showing the first resonance mode of the scanner in the vertical direction at 33 kHz (trampoline mode).

principle," i.e., for each scanning direction two pairs of piezos, which are of opposite phase with each other, are integrated in the scanner's flexure system in order to form a balanced structure (see Fig. 1). This has three main advantages: 1) the actuation is mechanically balanced, i.e., the recoil into the supporting structure gets minimized; 2) one piezo pushes while the other contracts, thus providing a higher force for actuation; and 3) the arrangement of the piezos is thermally balanced, which minimizes the thermal drift for stable imaging at highest resolution. Furthermore this also allows the implementation of a strain gauge full-bridge circuit that is also thermally balanced and can be used for closed-loop control of the scanning motion.

B. Finite-Element Analysis (FEA) and Implementation

The actual design of the scanner has been optimized using FEA tools (ANSYS, Canonsburg, PA). The predicted first resonance frequency in the scanning directions is at 27 kHz. Fig. 2 shows the first mode in the Z -direction (at 33 kHz), which is the sixth resonance mode of the scanner and is referred to in this paper as trampoline mode. Aluminum is used as the center piece and flexure material and a steel base housing serves as a rigid support of the piezos and flexures.

The push-pull structure in the X -direction is comprised of four piezo stack actuators with dimensions of $5 \times 5 \times 10 \text{ mm}^3$ and a nominal unloaded positioning range of $9 \mu\text{m}$ (AE0505D08, Tokin-NEC, Sendai City, Japan). The same assembly is implemented for actuation in the Y -direction. This symmetric design allows for full image rotation when imaging with the AFM, i.e., the fast scanning direction can be chosen arbitrarily in the X - Y -plane. A piezo stack actuator with dimensions of $2 \times 3 \times 5 \text{ mm}^3$ and an unloaded nominal range of $4.3 \mu\text{m}$ (AE0203D04, Tokin-NEC) is glued on the center piece to perform the actuation in the Z -direction. A photograph of the fully assembled scanner is given in Fig. 3. The positioning

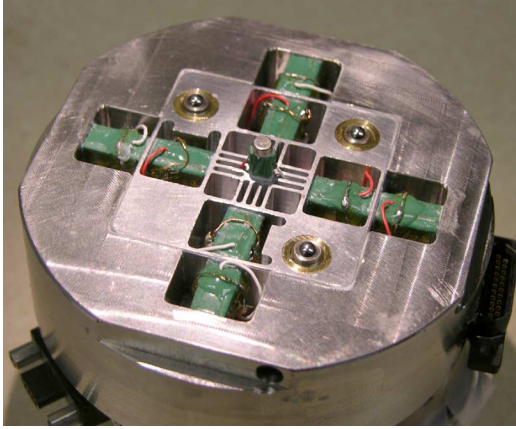


Fig. 3. Photograph of the high-speed scanner showing the eight scanning piezos integrated in the flexure system and the Z -piezo sitting on top of the center piece. The three screws sticking out of the flat top of the scanner are to approach the AFM-head including the cantilever onto the sample surface.

range of this scanner is $13 \mu\text{m}$ in the X - and Y -directions, and $4.3 \mu\text{m}$ in the Z -direction.

The piezo stacks are driven by custom made amplifiers (Tech-Project, Vienna, Austria) that have been designed for the specific capacitive load in order to achieve a high-positioning bandwidth. The driving voltage of the piezos is between 0 and 150 V. A 75-V offset is applied to all piezos to drive them symmetrically around this start position. The scanning signals are generated by a custom-made data acquisition system [9] that also records the AFM images.

III. MATHEMATICAL MODELING

Linear and nonlinear piezo dynamics have been studied extensively in literature. Specifically, hysteresis of the piezo actuator has been modeled (see [28] and the references therein) and compensated by inversion-based approaches [5]. Creep of the piezo material can be modeled [29] and, together with the hysteresis, compensated by open-loop [5] or feedback control (e.g., [19]). It has been reported that the piezo hysteresis does not affect the dynamics [5]. Even if the mechanical properties are not influenced by the hysteresis of the piezo, the system gain may depend on the operating conditions. These gain variations may be important for calibration and control design.

The dynamics of piezo positioners have been determined by physical modeling using partial differential equations [30], system identification [7], and frequency response [18], [20].

Physical modeling based on partial differential equations and finite-element modeling gives a physics-based high fidelity representation of the system, but the mathematical model is of too high order to be used for control.

System identification [31] based on measured sets of input and output data obtained from exciting the scanner with pseudo random binary data (PRBS) gives a good fit to the measured data [6], [23], but provides little physical insight.

In this paper, we have measured the frequency response directly. This is a fast and accurate method for systems with weakly damped resonances at high frequencies.

This section presents simplified mathematical models of the scanner that explains the dynamics of the system along the

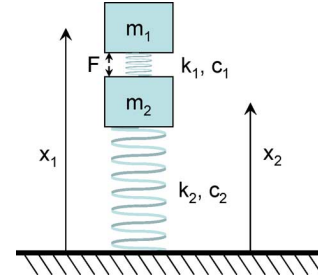


Fig. 4. Model of the scanner in the vertical direction. m_1 = half mass of the Z -piezo; k_1 = stiffness and c_1 = damping of the Z -piezo. m_2 = half mass of the Z -piezo plus effective mass of the supporting structure; k_2 = effective stiffness and c_2 = damping of the supporting structure. F is the force generated by the piezo and is regarded as the system input. The position x_1 is the system output.

vertical positioning axis. The essential dynamics of this system consists of the Z -actuator (driven by the power amplifier) and its interaction with the supporting structure. The derived model is of low order, gives physical insight, and is useful for both process and control design. The scanner is a complicated mechanical system with many oscillatory modes. We start by developing a simple mathematical model of second order that captures only the slowest mode [32]. This mode, which is called the trampoline mode, represents the vertical oscillation of the scanner against the elasticity in the support (flexures), (see Fig. 2). The insight and understanding obtained from this model is useful both for process design and for control design. The second-order model neglects the dynamics of the piezo stack. A fourth-order model that also includes the first mode of the Z -piezo is presented as well. This model, which is validated against measured frequency responses, is suitable for design of simple PI controllers, as well as more complicated model-based controllers.

A. Second-Order Model

Both the second- and the fourth-order models can be represented by the schematic diagram shown in Fig. 4. The vertical motion of the scanner system is modeled by two masses supported by a spring with damping.

The mass m_1 is the upper half of the Z -piezo plus the mass of the sample, m_2 is the lower half of the Z -piezo lumped with the effective mass of the supporting structure, which has the effective spring constant k_2 , and the effective damping coefficient c_2 . Parameter k_1 is the effective spring constant of the Z -piezo and c_1 are the corresponding effective damping coefficients. The piezo is assumed to exert the force F between the masses m_1 and m_2 . In the second-order model the spring k_1 is assumed to be infinitely stiff and the elongation of the spring is taken as the input.

Let the positions of the center of the masses be x_1 and x_2 . The elongation of the piezo stack is $\ell = x_1 - x_2$. Let the reaction force created by elongation of the piezo stack be F . A momentum balance gives the following model for the system:

$$\begin{aligned} m_1 \frac{d^2 x_1}{dt^2} &= F \\ m_2 \frac{d^2 x_2}{dt^2} &= -c_2 \frac{dx_2}{dt} - k_2 x_2 - F \\ \ell &= x_1 - x_2. \end{aligned}$$

Taking Laplace transforms gives

$$\begin{aligned} X_1(s) &= \frac{1}{m_1 s^2} F(s) \\ X_2(s) &= -\frac{1}{m_2 s^2 + c_2 s + k_2} F(s) \\ L(s) &= X_1(s) - X_2(s) \end{aligned}$$

and we get

$$\begin{aligned} L(s) &= X_1(s) - X_2(s) \\ &= \left(\frac{1}{m_1 s^2} + \frac{1}{m_2 s^2 + c_2 s + k_2} \right) F(s) \\ &= \frac{(m_2 + m_1)s^2 + c_2 s + k_2}{m_1 s^2 (m_2 s^2 + c_2 s + k_2)} F(s). \end{aligned}$$

When the dynamics of the piezo stack is neglected it is natural to consider the elongation of the stack as the input. The transfer function $G(s)$ from elongation $L(s)$ to position of the top of the stack $X_1(s)$ is

$$\begin{aligned} G(s) &= \frac{m_2 s^2 + c_2 s + k_2}{(m_2 + m_1)s^2 + c_2 s + k_2} \\ &= \frac{\alpha s^2 + 2\zeta\omega_0 s + \omega_0^2}{s^2 + 2\zeta\omega_0 s + \omega_0^2}. \end{aligned} \quad (1)$$

The transfer function is characterized by the following three parameters:

- resonance frequency $\omega_0 = \sqrt{k_2/(m_1 + m_2)}$ of the total mass oscillating against the spring;
- relative damping $\zeta = 0.5c_2/\sqrt{k_2(m_1 + m_2)}$;
- parameter $\alpha = m_2/(m_1 + m_2)$ which is determined by the ratio of the masses.

These parameters can be determined from a step response. Frequency and relative damping can be obtained from period and damping, parameter α from the initial and final values of the step. Let $h(t)$ be the step response of the transfer function given by (1). It follows from the initial and final value theorems for the Laplace transform that

$$\alpha = \frac{h(0)}{h(\infty)} = \frac{G(\infty)}{G(0)}. \quad (2)$$

Examples of step responses for different parameters are shown in Fig. 5.

More accurate modeling can be obtained from the frequency response. The Bode plots of the transfer function are shown in Fig. 6.

We have

$$G(i\omega_0) = 1 - i\frac{1-\alpha}{2\zeta}$$

for small ζ the peak of the frequency response occurs approximately at ω_0 and we have

$$|G(i\omega_0)| = \sqrt{1 + \frac{(1-\alpha)^2}{4\zeta^2}}. \quad (3)$$

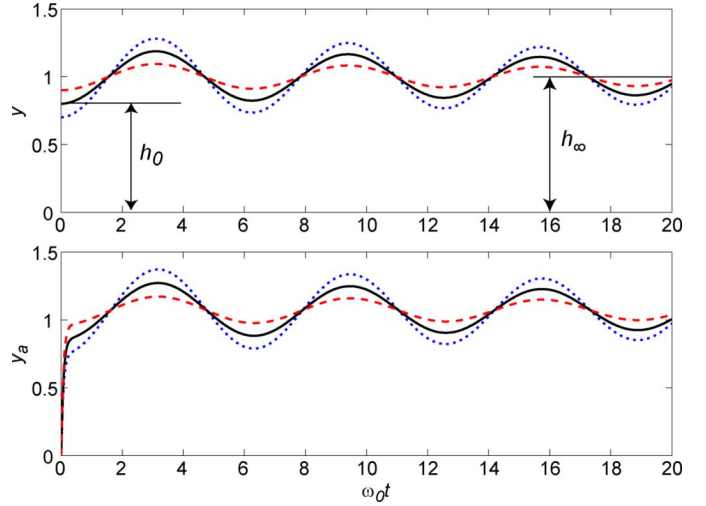


Fig. 5. Upper curves: Simulated step response of the scanner in Z -direction for $\zeta = 0.02$ and $\alpha = 0.7$ (dotted blue line), 0.8 (solid black line) and 0.9 (dashed red line). The lower curves show the step response when a time constant of the piezo amplifier of $\tau = 0.07/\omega_0$ is added.

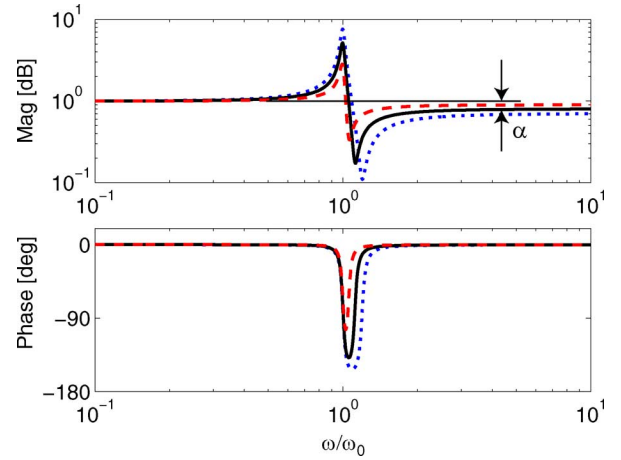


Fig. 6. Bode plot of the scanner model in Z -direction for $\zeta = 0.02$ and $\alpha = 0.7$ (dotted blue line), 0.8 (solid black line), and 0.9 (dashed red line).

For small ζ the dip in the frequency response occurs approximately at $\omega_0/\sqrt{\alpha}$ and we have

$$\left| G\left(i\frac{\omega_0}{\sqrt{\alpha}}\right) \right| = \left| \frac{2\zeta i}{\sqrt{\alpha} - \frac{1}{\sqrt{\alpha}} + 2\zeta i} \right| \approx \frac{2\zeta\sqrt{\alpha}}{1-\alpha}. \quad (4)$$

For $\alpha = 0.8$ and $\zeta = 0.02$ the resonance peak is 5.17 (5.10) at $\omega = 0.9977\omega_0$ (1.000) and the dip is 0.173 (0.179) at $\omega = 1.125\omega_0$ (1.118), where the approximate values are given in parentheses, according to (3) and (4).

The rapid drop in phase at the trampoline mode may limit the bandwidth that can be achieved with simple PI control, therefore, it is useful to have an estimate of this drop. The lowest phase occurs approximately at $\omega_0/\sqrt[4]{\alpha}$ and we have

$$G\left(i\frac{\omega_0}{\sqrt[4]{\alpha}}\right) = -\frac{[(1-\sqrt{\alpha})^2 - 4\zeta^2]\sqrt{\alpha} + 2\zeta i(1-\alpha)\sqrt[4]{\alpha}}{(1-\sqrt{\alpha})^2 + 4\zeta^2\sqrt{\alpha}}. \quad (5)$$

We thus obtain the following estimate of the largest phase drop:

$$\arg G\left(i\frac{\omega_0}{\sqrt{\alpha}}\right) = -\frac{\pi}{2} - \arctan \frac{[(1 - \sqrt{\alpha})^2 - 4\zeta^2]\sqrt{\alpha}}{2\zeta(1 - \alpha)}.$$

For $\alpha = 0.8$ and $\zeta = 0.02$ the smallest phase is -138° . A proportional–integral (PI) controller that attempts to have bandwidths close to ω_0 , will thus have a phase margin of at most 42° . For $\alpha = 0.7$ the phase margin becomes even smaller down to 28° . From this point of view, it is desirable to have α close to one. The mass ratio thus has implications for controller design, which can be assessed using the simple formula (5).

B. Fourth-Order Model

The simple model (1) captures the trampoline mode, which describes the dynamics of the interaction of the piezo element with its support. A simple physical model that also accounts for the dynamics of the piezo element is developed in this section. To obtain this model, we proceed as we did for the second-order model and represent the piezo stack with two masses joined by a spring k_1 . The lower mass is lumped with the mass of the support and the system can then be represented by the schematic picture in Fig. 4. Since we will be accounting for the dynamics of the piezo stack, it is natural to use the force exerted by the piezo as the input. In the lumped model, the piezo effect is represented by a force F acting between the masses. Using the notation in Fig. 4 the equations of motion become

$$M\frac{d^2x}{dt^2} + C\frac{dx}{dt} + Kx = \begin{pmatrix} F \\ -F \end{pmatrix}$$

where the state vector is $x = (x_1, x_2)^T$ and

$$M = \begin{pmatrix} m_1 & 0 \\ 0 & m_2 \end{pmatrix}$$

$$C = \begin{pmatrix} c_1 & -c_1 \\ -c_1 & c_1 + c_2 \end{pmatrix}$$

$$K = \begin{pmatrix} k_1 & -k_1 \\ -k_1 & k_1 + k_2 \end{pmatrix}.$$

Taking Laplace transforms gives the following relation between piezo force F and displacement x_1

$$X_1(s) = \frac{m_2s^2 + c_2s + k_2}{D(s)}F(s)$$

$$X_2(s) = -\frac{m_1s^2}{D(s)}F(s) \quad (6)$$

where

$$D(s) = m_1m_2s^4 + (m_1(c_1 + c_2) + m_2c_1)s^3$$

$$+ (m_1(k_1 + k_2) + m_2k_1 + c_1c_2)s^2$$

$$+ (c_1k_2 + c_2k_1)s + k_1k_2$$

$$= m_1m_2(s^2 + 2\zeta_1\omega_1s + \omega_1^2)(s^2 + 2\zeta_3\omega_3s + \omega_3^2) \quad (7)$$

and

$$2(\zeta_1\omega_1 + \zeta_3\omega_3) = \frac{m_1(c_1 + c_2) + m_2c_1}{m_1m_2}$$

$$\omega_1^2 + 4\zeta_1\zeta_3\omega_1\omega_3 + \omega_3^2 = \frac{m_1(k_1 + k_2) + m_2k_1 + c_1c_2}{m_1m_2}$$

$$2(\zeta_1\omega_1\omega_3^2 + \omega_1^2\zeta_3\omega_3) = \frac{c_1k_2 + c_2k_1}{m_1m_2}$$

$$\omega_1^2\omega_3^2 = \frac{k_1k_2}{m_1m_2}.$$

The transfer function from force F to displacement x_1 is

$$G_{x_1F}(s) = \frac{m_2s^2 + c_2s + k_2}{D(s)}$$

$$= \frac{s^2 + 2\zeta_2\omega_2s + \omega_2^2}{m_1(s^2 + 2\zeta_1\omega_1s + \omega_1^2)(s^2 + 2\zeta_3\omega_3s + \omega_3^2)}. \quad (8)$$

The system has two resonances ω_1 and ω_3 and one anti-resonance ω_2 . The mode ω_1 is the trampoline mode and the mode ω_3 is the first resonant mode of the piezo. The anti-resonance is the same as for the second-order model. The mass m_1 is typically smaller than m_2 and the spring constant k_1 is typically much larger than k_2 , which gives the following approximations for the frequencies:

$$\omega_1 \approx \sqrt{\frac{k_2}{m_1 + m_2}}$$

$$\omega_2 = \sqrt{\frac{k_2}{m_2}}$$

$$\omega_3 \approx \sqrt{\frac{(m_1 + m_2)k_1}{m_1m_2}} = \sqrt{\frac{k_1}{\alpha m_1}}. \quad (9)$$

Notice that with these approximations, the frequencies ω_1 and ω_2 are the same as for the second-order model [see (1)]. Another way to see that the fourth-order model is compatible with the second-order model is to investigate what happens when the spring coefficient k_1 is large. We have

$$\lim_{k_1 \rightarrow \infty} \frac{k_1 X_1(s)}{F(s)} = \frac{m_2s^2 + c_2s + k_2}{(m_1 + m_2)s^2 + c_2s + k_2}$$

which is identical to the second-order model given by (1). The same is obtained when computing the transfer function from elongation $L(s)$ to displacement $X_1(s)$ for the fourth-order model. In this case, the spring k_1 would not be considered and overruled by the displacement $L(s)$ and we find that $G(s)$ is identical to the transfer function for the second-order system (1).

The mathematical model gives insight into the dynamics of the scanner, it contributes to a better understanding of system dynamics and it can be used for improved process design. The parameter m_1 represents half the mass of the Z -piezo plus the sample mass and is about 20% of the total mass for $\alpha = 0.8$. This means that for the Z -direction the effective mass of the supporting structure is about $1.5\times$ the mass of the Z -piezo. From (1), it can be seen that the transfer function is $G(s) = 1$ if $\alpha = 1$. From Figs. 5 and 6, it is seen that the larger α is, the smaller are the oscillations due to the Z -piezo support. Although using a heavier material or building the supporting structure in Z thicker might compromise the scanning motion by increasing the moved masses, it would increase the mass ratio α and, therefore, reduce the influence of its dynamics. However, since this behavior is known in advance, it also can be compensated for by utilizing modern model based control methods (cf. [23]), which may be the favorable choice in order not to compromise the dynamics in the scanning directions.

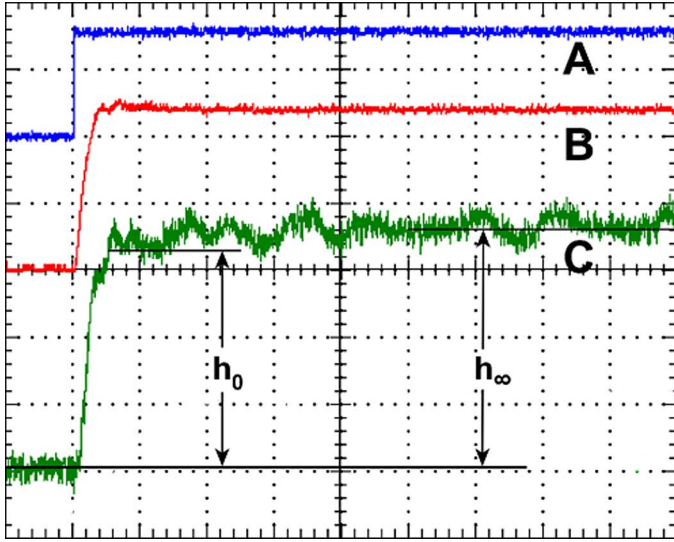


Fig. 7. Measured step response of the scanner in Z -direction. (A) Input step signal (blue, 50 mV/div). (B) Output of the power amplifier (red, 500 mV/div). (C) Z -position sensed by the cantilever (green, 200 mV/div). Time scale is 25 μ s/div. From h_0 and h_∞ the ratio of the masses can be determined. The data in the figure gives $\alpha = h_0/h_{\text{inf}} \approx 0.9$.

IV. MODEL VALIDATION

The real scanner is a complex electro-mechanical system with many resonant modes. The physics-based models derived in Section III contain simple low-order dynamics. In this section, we present experimental results that indicate that the simple models do indeed capture properties of the real scanner that are relevant for control design. Both step tests and frequency response techniques were used for the validation.

A. Step Responses

To measure the step response of the scanner, we considered the power amplifier for the Z -piezo as the input and the photo diode signal displaying the cantilever deflection as the output. A small piece of silicon was glued on top of the piezo as a standard specimen. The Z -position of the sample is sensed by the AFM cantilever operating in contact mode without scanning. The input steps are generated by a function generator (Agilent/HP 3311A, Palo Alto, CA). Fig. 7 shows a measured step response with an input step of 80 mV (Signal A). The signal is amplified by the power amplifier to 1.2 V (Signal B). This voltage is applied to the piezo and represents a nominal step height of 34 nm. The cantilever deflection is measured by the optical lever setup of the AFM using a custom-made high-bandwidth deflection electronics (Signal C). The experimental data are in good agreement with the mathematical model of the scanner derived in Section III. A quick analysis shows that there is a fast initial response followed by a poorly damped oscillation with a frequency around 40 kHz. A more detailed analysis gives a rise time of the voltage at the amplifier output (signal B) to be around 10 μ s. The time of the upward ramp in the cantilever deflection signal is about the same for the high-bandwidth deflection electronics (Signal C). The measured step response is in good agreement with the modeling and simulation shown in Fig. 5. The

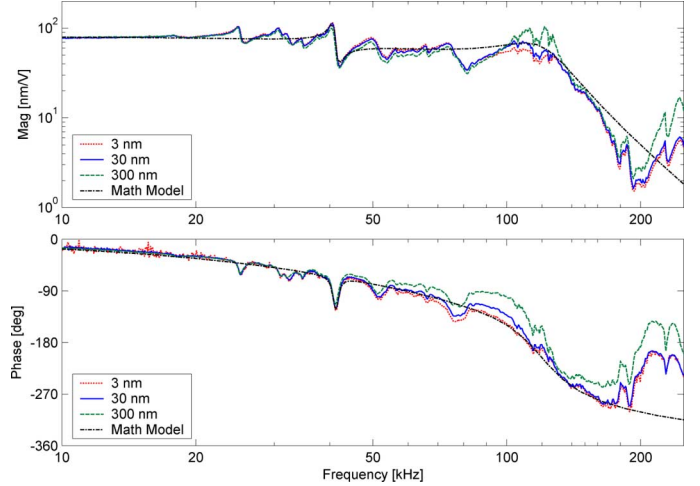


Fig. 8. Bode plot of the frequency response of the scanner in the Z -direction. The peak-to-peak excitation amplitudes are 3 nm (dotted red line), 30 nm (solid blue line), and 300 nm (dashed green line). A Bode plot of a fitted model is also shown (dash-dotted black line).

small and fast oscillations (see Fig. 7, Signal C) that are superimposed on the modeled oscillations are due to a higher mode, presumably the resonance of the Z -piezo at 120 kHz. Applying (2) to the data in Fig. 7 gives the mass-ratio $\alpha = h_0/h_{\text{inf}} \approx 0.9$.

B. Frequency Response

The frequency response of the transfer function from the input to the power amplifier to the vertical displacement of the piezo was also measured directly with a network analyzer (Agilent 4395A, Palo Alto, CA). The velocity of the top of the Z -piezo was measured by a laser Doppler vibrometer (OFV-3001, Polytec, Waldbronn, Germany). The sinusoidal frequency sweep with constant excitation amplitude is generated by the network analyzer. Using the vibrometer [33], we recorded velocity data of the piezo top during the frequency sweep. The velocity data was converted to position data dividing gain by frequency and subtracting 90° from the phase. The nominal time delay of the vibrometer of 1.9 μ s was also removed. The fact that the system can be modeled linearly is validated in Fig. 8, which shows the bode plot of the scanner system for excitation amplitudes covering two decades. For modeling typical AFM applications, the bode plot of the 30-nm excitation (solid blue line) will be used as the nominal system response.

The gain curve in Fig. 8 shows the resonance peak at about 40 kHz and the dip (anti-resonance) as modeled by (1) and shown in Fig. 6. The gain curve also shows a resonance at about 120 kHz, which is the resonance frequency of the piezo as modeled in (8), which is close to the nominal value specified by the piezo manufacturer. This also can be determined by the fact that at this resonance the low-pass characteristic of the actuator can be observed. The bode plot was used to fit the parameters of the mathematical model derived in Section III. A simple way to fit the model to the data is to start with the frequencies where the gain curve has its peaks. This gives the frequencies $f_1 = \omega_1/2\pi = 40.9$ kHz, $f_2 = \omega_2/2\pi = 41.6$ kHz, and $f_3 = \omega_3/2\pi = 120$ kHz. The relative dampings are then

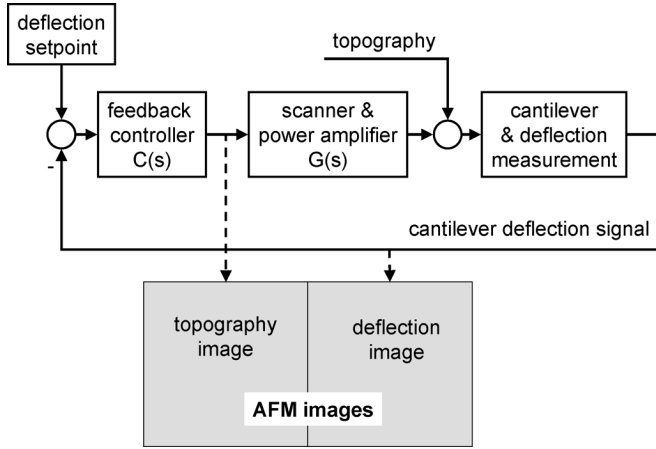


Fig. 9. Block diagram of the system for vertical positioning of the cantilever. The controller has transfer function $C(s)$ the power amplifier and the piezo has transfer function $G(s)$ and the laser beam and the photodetector is modeled by a constant gain. The output of the controller gives the topography image, the control error gives the deflection image.

adjusted to give the correct peaks, which gives $\zeta_1 = 0.016$, $\zeta_2 = 0.016$, and $\zeta_3 = 0.17$. To get a good fit, we also have to include the dynamics of the amplifier, which has been modeled by second-order dynamics with a frequency 74 kHz and a relative damping $\zeta = 1$. The results are shown with the dashed-dotted line in Fig. 8. The measured Bode plot indicates that there are additional zeros around 200 kHz. The gain for these frequencies are, however, very small, corresponding to motions of < 1 nm in the experiment. For control design, it is important to make sure that there is sufficient roll-off to deal with these zeros.

The multiple resonance and anti-resonance pairs between 22 and 35 kHz are attributed to the flexures for the X and Y movement, which agrees with the frequency range of the scanner resonances in the X - and Y -directions obtained from the FEA simulations. Between the anti-resonance at 41.6 kHz and the resonance of the piezo at 120 kHz one can observe additional resonance – anti-resonance pairings in the spectrum due to higher modes of the scanner, however, these peaks are not dominant in the frequency spectrum of the scanner in the Z -direction.

V. FEEDBACK CONTROL

In AFM imaging, the cantilever scans the sample horizontally and the vertical position is controlled to keep the cantilever deflection constant. The control system for the cantilever deflection has a major influence on the quality of the image. A schematic block diagram of the system is shown in Fig. 9. The tip of the cantilever is clamped to the sample surface by attractive van der Waals and repulsive Pauli forces [2], [34], while the other end of the cantilever is fixed in the frame of reference. The sample surface, being probed by the tip, is positioned by the Z -piezo. The controller attempts to keep a constant deflection of the cantilever, resulting in a constant force interaction between tip and sample. The set point of the controller is proportional to the force that is exerted on the sample. It is desirable to have a small force to avoid damaging the sample or tip.

The primary output of the system is an image of the sample. The topography image is formed from the controller output and the deflection image is formed from the cantilever deflection as

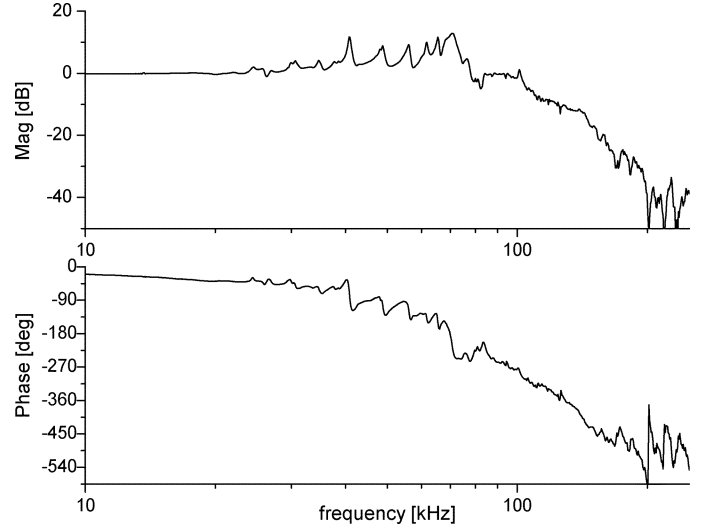


Fig. 10. Bode plot of the complementary sensitivity function with PI control. The peak-to-peak amplitude of the input signal corresponds to a deflection of 30 nm.

shown in Fig. 9. To see how the images are related, introduce the transfer functions of the controller $C(s)$ and the scanner and power amplifier $G(s)$. The cantilever deflection is modeled simply by its deflection sensitivity d_s , which is assumed constant. Let the topography be denoted by v . Taking the Laplace transform, we find that the controller output is given by

$$\begin{aligned} U(s) &= G_{uv}(s)V(s) \\ &= \frac{C(s)d_s}{1 + G(s)C(s)d_s}V(s) \\ &= \frac{T(s)}{G(s)}V(s) \end{aligned}$$

where $T(s)$ is the complementary sensitivity function of the feedback loop. The cantilever deflection signal is given by

$$\begin{aligned} Y(s) &= G_{yv}(s)V(s) \\ &= \frac{d_s}{1 + G(s)C(s)d_s}V(s) \\ &= d_s S(s)V(s) \end{aligned}$$

where $S(s)$ is the sensitivity function of the feedback loop. A good topography image is obtained if the transfer function $G_{uv}(s)$ has constant gain over a wide frequency range.

In our prototype system, the controller is an analog PI controller. In the measurements shown in this paper, the controller is tuned empirically, with the starting value of integral gain slightly below the critical value [35]. Both proportional and integral gain are iteratively increased to get a high bandwidth without ringing of the feedback loop. Fig. 10 shows a complementary sensitivity function $T(s)$, which is measured with the network analyzer (Agilent 4395A). The AFM system is operated in contact mode without scanning. In order to avoid observation of the cantilever dynamics, a stiff cantilever (Model: RTEPW, Veeco Instruments Inc., Woodbury, NY) with a nominal spring constant of $k = 40$ N/m and a free resonance frequency of $f_0 = 358$ kHz is used. The feedback loop (cf. Fig. 9) is excited by

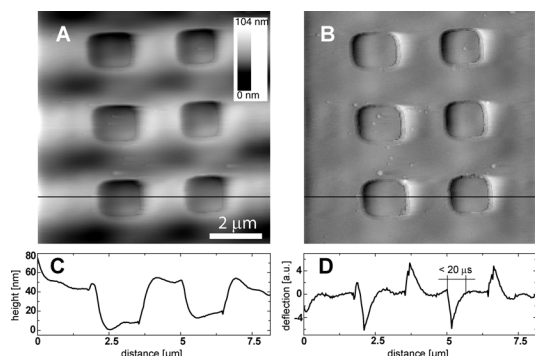


Fig. 11. Silicon calibration grating, imaged at 2060 lines/s with the high-speed AFM, showing 44-nm deep etched holes with a pitch of 3 μ m. (A) topography image. (B) Cantilever deflection. (C) Cross section of topography marked in (A). (D) Cross section of the cantilever deflection marked in (B).

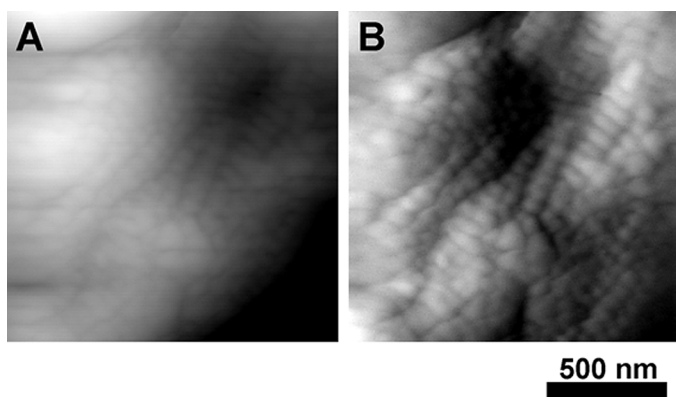


Fig. 12. Natural surface of a single trabecula from a bovine femur, imaged at 2060 lines/s with the high-speed AFM, showing collagen fibrils with the typical 67-nm banding pattern. (A) Topography image. (B) Cantilever deflection. Color scaling in (A) is 100 nm from black to white.

adding the network analyzer output signal to the cantilever deflection. This is done using a custom made summing amplifier and corresponds to changing the set point. The system response, given by the cantilever deflection, is connected to the input of the network analyzer.

An analysis of the transfer functions in Figs. 8 and 10 shows that the transfer function $G_{uw}(s)$ has a gain that is reasonably constant up to frequencies of about 100 kHz, which explains the good resolution of the images in Figs. 11 and 12. The image can be improved even further by combining the topography and deflection images using model-based control. Design of such controllers will be discussed elsewhere, let it suffice to mention that the physics-based models developed in this paper are well suited for control design and also that the traditional tradeoffs between performance and robustness will have a stronger emphasis on performance since the operator typically adjusts the controller for each measurement, based on the obtained images. The operation of the instrument can also be simplified by introducing facilities for automatic tuning of the controller.

VI. IMAGING RESULTS

To demonstrate the performance of our high-speed AFM system a silicon calibration grating and a biological specimen

are imaged at a scan-rate of 2060 lines/s and a resolution of 256 \times 256 pixels². This corresponds to a scan speed of 8 frames/s.

The high-speed images are recorded with a custom DAQ-system [9] that also generates the scanning signals for the movement in the X - and Y -directions. The first resonance frequencies of the scanner in the scanning directions occur at 22 kHz. For imaging at high-speed, lateral oscillations of the scanner have been compensated by an input shaping approach [36]. Besides the fact that coupling between the scanning axis and the Z -direction gets suppressed by the inner frame, this compensation of the lateral dynamics also minimizes any imaging artifacts due to the residual coupling between the scanning directions and the Z -direction. In order to demonstrate the high-speed imaging capability of this scanning unit, no clipping of the images on the sides has been applied to hide turn-around artifacts, i.e., the full width of the recorded images is presented.

Fig. 11 shows a silicon calibration grating recorded with the high-speed AFM at 2060 lines/s in contact mode with a soft, small cantilever ($k < 0.1$ N/m, $f_0 = 207$ kHz, SCL-Sensor.Tech., Deutsch-Wagram, Austria). The tip sample interaction force is held constant by the analogue PI feedback controller tuned by the AFM user. Both the topography image, representing the output of the feedback controller (cf. Fig. 9), and the cantilever deflection, being the residual control error, are displayed. These images demonstrate that the feedback controller is able to track the surface at high-speed since variations in the deflection image (B) occur only around the edges of the grating, while the cantilever deflection is mostly constant on the flat areas of the sample. In the topography image (A), the holes of the grating clearly can be seen. The additional brighter and darker areas also visible in image (A) are due to interference of the laser from the optical lever setup on reflecting samples, generating artifacts in the measured cantilever deflection, which will be eliminated in future prototypes of the high-speed AFM. Image (C) shows a cross section of the topography, marked by the black line in image (A). From the cross section (D) of the cantilever deflection, marked in (B), the settling time of the user adjusted feedback system in response to a step like change in the surface can be estimated to be less than 20 μ s.

Fig. 12 shows AFM images of the surface of a single bone trabecula from a bovine bone femur, also recorded in contact mode with a soft, small cantilever ($k < 0.1$ N/m, $f_0 > 200$ kHz). Collagen fibrils of about 100 nm in diameter with the typical corrugation-periodicity of 67 nm [37] can clearly be seen. The topography image has been improved in contrast by using unsharp masking, in order to display the fine topographical details of the banding pattern more clearly, which are small as compared to the overall topography of the bone surface.

Although the fine topographical details can be seen better in the deflection image, it is crucial to make the feedback bandwidth as high as possible. This minimizes variations in the tip-sample interaction force and avoids damage to biological specimens that are more fragile than the sample shown in Fig. 12. The high bandwidth requirement arises from the fact, that the spatial frequencies of the sample topography are transformed into the time domain via the imaging speed. If the tip travels at higher speed over the sample surface, topographical changes occur much faster to the tip. In order to keep variations of the

imaging force low, the feedback controller correspondingly also has to react much faster. The fact that the feedback controller still reacts at the high speed (5.6 mm/s) is evident by the fine topographical features that can be seen in the topography image.

VII. CONCLUSION

In this paper, we present the design and a simplified mathematical model of a high-speed scanner for an atomic force microscope. A guiding theme for this project has been the development of a high-performance system by combined process and control design. A physics-based model is essential because it gives the possibilities to understand how process design influences control design. We focus here on the modeling, the control design will be discussed elsewhere.

The fourth-order model obtained from first principles explains the main dynamics of the scanner in the vertical direction and gives insight into the interplay of design parameters, such as the ratio of the masses α . Experimental step responses and frequency spectra verify the mathematical model and give quantitative values of some unknown parameters of the mathematical model. For future prototype designs, these model parameters will help to optimize the system dynamics during the design of the scanner for highest speed and positioning accuracy. Furthermore, this model is a good basis to implement a model-based controller, that can compensate the higher-order dynamics of the high-speed scanner, in order to reduce the residual control error and to further improve the image quality. Additionally, this will allow for implementation of an observer [7], [27] for more accurate conversion of the control action into the topography signal.

Finally, the vertical positioning axis is discussed in terms of PI feedback control and the performance of the AFM system is demonstrated by images of a calibration grating and a biological specimen recorded at high-speed.

REFERENCES

- [1] G. Binnig, C. Quate, and C. Gerber, "Atomic force microscope," *Phys. Rev. Lett.*, vol. 56, no. 9, pp. 930–933, 1986.
- [2] D. Sarid, *Scanning Force Microscopy*. New York: Oxford Univ. Press, 1994.
- [3] S. Alexander, L. Helleman, O. Marti, J. Schneir, V. Elings, P. Hansma, M. Longmire, and J. Gurley, "An atomic-resolution atomic force microscope implemented using an optical lever," *J. Appl. Phys.*, vol. 65, pp. 164–167, 1989.
- [4] T. Sulchek, G. Yaralioglu, C. Quate, and S. Minne, "Characterization and optimization of scan speed for tapping-mode atomic force microscopy," *Rev. Sci. Instrum.*, vol. 73, no. 8, pp. 2928–2936, 2002.
- [5] D. Croft, G. Shed, and S. Devasia, "Creep, hysteresis, and vibration compensation for piezoactuators: Atomic force microscopy application," *ASME J. Dyn. Syst., Meas., Control*, vol. 123, pp. 35–43, 2001.
- [6] G. Schitter and A. Stemmer, "Identification and open-loop tracking control of a piezoelectric tube scanner for high-speed scanning probe microscopy," *IEEE Trans. Control Syst. Technol.*, vol. 12, no. 3, pp. 449–454, May 2004.
- [7] G. Schitter, P. Menold, H. Knapp, F. Allgöwer, and A. Stemmer, "High performance feedback for fast scanning atomic force microscopes," *Rev. Sci. Instrum.*, vol. 72, no. 8, pp. 3320–3327, 2001.
- [8] A. Humphris, J. Hobbs, and M. Miles, "Ultrahigh-speed scanning near-field optical microscope capable of over 100 frames per second," *Appl. Phys. Lett.*, vol. 83, no. 1, pp. 6–8, 2003.
- [9] G. Fantner, P. Hegarty, J. Kindt, G. Schitter, G. Cidade, and P. Hansma, "Data acquisition system for high speed atomic force microscopy," *Rev. Sci. Instrum.*, vol. 76, no. 2, p. 026118, 2005.
- [10] D. Walters, J. Cleveland, N. Thomson, M. Wendman, G. Gurley, V. Elings, and P. K. Hansma, "Short cantilevers for atomic force microscopy," *Rev. Sci. Instrum.*, vol. 67, no. 10, pp. 3583–3590, 1996.
- [11] M. Viani, T. Schaffer, A. Chand, M. Rief, H. Gaub, and P. Hansma, "Small cantilevers for force spectroscopy of single molecules," *J. Appl. Phys.*, vol. 86, no. 4, pp. 2258–2262, 1999.
- [12] S. Manalis, S. Minne, and C. Quate, "Atomic force microscopy for high speed imaging using cantilevers with an integrated actuator and sensor," *Appl. Phys. Lett.*, vol. 68, no. 6, pp. 871–873, 1996.
- [13] T. Sulchek, S. C. Minne, J. D. Adams, D. A. Fletcher, A. Atalar, C. F. Quate, and D. M. Adderton, "Dual integrated actuators for extended range high speed atomic force microscopy," *Appl. Phys. Lett.*, vol. 75, no. 11, pp. 1637–1639, 1999.
- [14] T. Ando, N. Kodera, E. Takai, D. Maruyama, K. Saito, and A. Toda, "A high-speed atomic force microscope for studying biological macromolecules," *Proc. Nat. Acad. Sci. USA*, pp. 12468–12472, 2001.
- [15] J. Kindt, G. Fantner, J. Cutroni, and P. Hansma, "Rigid design of fast scanning probe microscopes using finite element analysis," *Ultramicroscopy*, vol. 100, no. 3–4, pp. 259–265, 2004.
- [16] M. Rost, L. Crama, P. Schakel, E. van Tol, G. van Velzen-Williams, C. Overgaw, H. ter Horst, H. Dekker, B. Okhuijsen, M. Seynen, A. Vijftigschild, P. Han, A. Katan, K. Schoots, R. Schumm, W. van Loo, T. Oosterkamp, and J. Frenken, "Scanning probe microscopes go video rate and beyond," *Rev. Sci. Instrum.*, vol. 76, p. 053710, 2005.
- [17] A. Humphris, M. Miles, and J. Hobbs, "A mechanical microscope: High-speed atomic force microscopy," *Appl. Phys. Lett.*, vol. 86, no. 3, p. 034106, 2005.
- [18] D. Croft and S. Devasia, "Vibration compensation for high speed scanning tunneling microscopy," *Rev. Sci. Instrum.*, vol. 70, no. 12, pp. 4600–4605, 1999.
- [19] S. Salapaka, A. Sebastian, J. Cleveland, and M. Salapaka, "High bandwidth nano-positioner: A robust control approach," *Rev. Sci. Instrum.*, vol. 73, no. 9, pp. 3232–3241, 2002.
- [20] A. Sebastian and S. Salapaka, "Design methodologies for robust nano-positioning," *IEEE Trans. Control Syst. Technol.*, vol. 13, no. 6, pp. 868–876, Nov. 2005.
- [21] A. Fleming and S. Moheimani, "Sensorless vibration suppression and scan compensation for piezoelectric tube nanopositioners," *IEEE Trans. Contr. Syst. Technol.*, vol. 14, no. 1, pp. 33–44, Jan. 2006.
- [22] Q. Zou, K. Leang, E. Sadoun, M. Reed, and S. Devasia, "Control issues in high-speed afm for biological applications: Collagen imaging example," *Asian J. Control*, vol. 6, no. 2, pp. 164–178, 2004.
- [23] G. Schitter, A. Stemmer, and F. Allgöwer, "Robust two-degree-of-freedom control of an atomic force microscope," *Asian J. Control*, vol. 6, no. 2, pp. 156–163, 2004.
- [24] K. El Rifai, O. El Rifai, and K. Youcef-Toumi, "On dual action in atomic force microscopes," in *Proc. IEEE Amer. Control Conf.*, 2004, pp. 3128–3133.
- [25] S. Minne, S. Manalis, and C. Quate, "Parallel atomic force microscopy using cantilevers with integrated piezoresistive sensors and integrated piezoelectric actuators," *Appl. Phys. Lett.*, vol. 67, no. 26, pp. 3918–3920, 1995.
- [26] E. Eleftheriou, T. Antonakopoulos, G. Binnig, G. Cherubini, M. Despont, A. Dholakia, U. Durig, M. Lantz, H. Pozidis, H. Rothuizen, and P. Vettiger, "Millipede—A MEMs-based scanning-probe data-storage system," *IEEE Trans. Magn.*, vol. 39, no. 2, pp. 938–945, Mar. 2003.
- [27] S. Salapaka, T. De, and A. Sebastian, "Sample-profile estimate for fast atomic force microscopy," *Appl. Phys. Lett.*, vol. 87, p. 053112, 2005.
- [28] R. Smith, S. Seelecke, M. Dapino, and Z. Ounaies, "A unified framework for modeling hysteresis in ferroic materials," *J. Mechan. Phys. Solids*, vol. 54, pp. 46–85, 2006.
- [29] H. Jung, J. Shim, and D. Gweon, "Tracking control of piezoelectric actuators," *Nanotechnol.*, vol. 12, no. 1, pp. 14–20, 2001.
- [30] H. Adriaens, W. deKoning, and R. Banning, "Modeling piezoelectric actuators," *IEEE Trans. Mechatron.*, vol. 5, no. 4, pp. 331–341, Dec. 2000.
- [31] L. Ljung, *System Identification, Theory for the User*, T. Kailath, Ed., 2nd ed. Upper Saddle River, NJ: PTR Prentice-Hall, 1999, Information and System Sciences Series.
- [32] G. Schitter, K. Åström, B. DeMartini, G. Fantner, K. Turner, P. Thurner, and P. Hansma, "Design and modeling of an high-speed scanner for atomic force microscopy," in *IEEE Proc. Amer. Control Conf.*, 2006, pp. 502–507.
- [33] K. Turner, P. Hartwell, and N. MacDonald, "Multi-dimensional MEMS motion characterization using laser vibrometry," in *Dig. Techn. Papers, Transducers 10th Int. Conf. Solid-State Sens. Actuators*, 1999, pp. 144–147.

- [34] R. Stark, G. Schitter, M. Stark, R. Guckenberger, and A. Stemmer, "State-space model of freely vibrating and surface-coupled cantilever dynamics in atomic force microscopy," *Phys. Rev. B*, vol. 69, p. 085412, 2004.
- [35] K. J. Åström and T. Häggglund, *Advanced PID Control*. Research Triangle Park, NC: ISA—The Instrumentation, Systems, and Automation Society, 2005.
- [36] G. Schitter, G. Fantner, P. Thurner, J. Adams, and P. Hansma, "Design and characterization of a novel scanner for high-speed atomic force microscopy," in *Proc. 4th IFAC Symp. Mechatron.*, 2006, pp. 819–824.
- [37] T. Hassenkam, G. Fantner, J. Cutroni, J. Weaver, D. Morse, and P. Hansma, "High-resolution afm imaging of intact and fractured trabecular bone," *Bone*, vol. 35, no. 1, pp. 4–10, 2004.



Barry E. DeMartini (M'05) received the B.S. degree in mechanical engineering from the University of California, Santa Barbara, in 2003, where he is currently pursuing the Ph.D. degree in mechanical engineering.

His research interests include resonant mass sensors for chemical and biological detection, design and characterization of micro/nanoscale resonators, and nonlinear dynamics and chaos in microelectromechanical systems.



Philipp J. Thurner received the M.Sc. degree in physics from the Graz University of Technology, Graz, Austria, in 1999 and the Ph.D. degree in biomedical engineering and materials science from the Swiss Federal Institute of Technology, the Swiss Federal Laboratories for Materials Testing and Research, Zurich, Switzerland, in 2004.

He is currently starting a position at the University of California, San Francisco. From 2004 to 2006 he was a Postdoctoral Fellow with the University of California, Santa Barbara. His main research interest

is in functional imaging of calcified tissue structure and in calcified tissue mechanics from the macro- to the nanoscale.

Dr. Thurner is a member of the Deutsche Physikalische Gesellschaft (DPG), the American Physical Society (APS), the Materials Research Society (MRS), the Materials Research Society Singapore (MRS), the International Society for Bone and Mineral Research (IBMS), the Austrian Society for Bone and Mineral Research (AuSBMR), and the Biophysical Society (BPS).



Georg Schitter (M'05) received the M.Sc. degree in electrical engineering from the Graz University of Technology, Graz, Austria, in 2000, the M.Sc. degree in information technology, and the Ph.D. degree in technical sciences from the Swiss Federal Institute of Technology Zurich, Zurich, Switzerland, in 2004.

He is currently an Assistant Professor with the Delft University of Technology, the Delft Center for Systems and Control, Delft, The Netherlands. He was a Project Scientist with the Paul Hansma Laboratory, University of California Santa Barbara,

Santa Barbara, from 2004 to 2006. His primary research interests include mechanical design and model-based control of mechatronic and microsystems, in particular for high-precision positioning and scanning probe microscopy applications.

Dr. Schitter was a recipient of four awards and has been granted three prestigious fellowships. He is a member of the American Society of Mechanical Engineers (ASME) and the American Physical Society (APS).



Karl J. Åström (F'07) received the M.Sc. and Ph.D. degrees from the Royal Institute of Technology, Stockholm, Sweden.

He is currently a Visiting Professor with the University of California, Santa Barbara (UCSB) and he has held visiting appointments at many universities in the United States, Europe, and Asia. In 1965, he became a Professor of Automatic Control with Lund University, Lund, Sweden, where he built the Department of Automatic Control.

Prof. Åström is a fellow of IFAC and a member of the Royal Swedish Academy of Sciences, and the Royal Swedish Academy of Engineering Sciences (IVA), where he has also been a Vice President. He is a Foreign Associate of the U.S. National Academy of Engineering. He was a recipient of many awards, including the Rufus Oldenburger Medal from the ASME in 1985, the Quazza Medal from IFAC in 1987, the IEEE Control Systems Science and Engineering Award in 1990, and the IEEE Medal of Honor in 1993.



Kimberly L. Turner received the B.S. degree in mechanical engineering from Michigan Technological University, Houghton, in 1994 and the Ph.D. degree in theoretical and applied mechanics from Cornell University, Ithaca, NY, in 1999.

She is currently an Associate Professor of mechanical and environmental engineering with the University of California, Santa Barbara, where she has served on the faculty since 1999. Her research interests include nonlinear dynamics of micro/nanoscale systems, testing and characterization of MEMS devices, modeling of micro/nanoscale devices, and solid-state sensor development.

Dr. Turner is a Member of American Society of Mechanical Engineers (ASME), SEM, AVS, and the Cornell Society of Engineers. She was a recipient of the National Science Foundation CAREER Award and the Varian Award from the AVS.



Paul K. Hansma received the B.A. degree from New College, Sarasota, FL, and the M.A. and Ph.D. degrees from the University of California, Berkeley (UCSB).

He joined the Physics Department, UCSB, in 1972 as an Assistant Professor, became an Associate Professor in 1976, and attained full professorship in 1980. He pioneered instrumentation for scanning probe microscopy, in particular atomic force microscopy, for 25 years, and he holds several key patents in this field. In his research, the development

of better instruments is driven by challenging applications in bio-physics and material science.

Prof. Hansma was a recipient of the distinguished Biological Physics Prize in 2000 from the American Physical Society.